Fractal dimension of diffusion-limited aggregation clusters grown on spherical surfaces

J. M. Tenti, S. N. Hernández Guiance, and I. M. Irurzun*

Facultad de Ciencias Exactas, Instituto de Investigaciones Fisicoquímicas Teóricas y Aplicadas, CCT La Plata, Universidad Nacional de La Plata, B1904 La Plata, Buenos Aires, Argentine Republic

(Received 11 June 2020; accepted 4 January 2021; published 29 January 2021)

In this work we study the fractal properties of diffusion-limited aggregation (DLA) clusters grown on spherical surfaces. Diffusion-limited aggregation clusters, or DLA trees, are highly branched fractal clusters formed by the adhesion of particles. In two-dimensional media, DLA clusters have a fractal dimension $D_f = 1.70$ in the continuous limit. In some physical systems, the existence of characteristic lengths leads us to model them as discrete systems. Such characteristic lengths may result also from limitations in measuring instruments, for example, the resolution of biomedical imaging systems. We simulate clusters for different particle sizes and examine the influence of discretization by exploring the systems in terms of the relationship between the particle size r and the radius of the sphere R. We also study the effect of stereographic projection on the fractal properties of DLA clusters. Both discretization and projection alter the fractal dimension of DLA clusters grown on curved surfaces and must be considered in the interpretation of photographic biomedical images.

DOI: 10.1103/PhysRevE.103.012138

I. INTRODUCTION

Fractal geometry can be used to characterize natural objects [1]. Coastlines are classic examples of fractal objects [2]. Fractal shapes are scale independent and self-similar objects with a representative fractal dimension D_f. This parameter has been used in some recent studies on biomedical imaging, for example, for pattern recognition in stained cell images [3] or for retinal vascular fractal analysis, using digital retina images [4]. The distribution of biophysical parameters obtained by reconstructing a phase space can provide a statistically significant assessment of breast tumor grade, a factor that indicates the degree of malignancy of the tumor [5]. To understand the abnormalities in the cerebellum of Chiari type I malformation patients, the fractal dimension of the region has been used as a discriminative feature [6]. Fractal dimensions have also been used to characterize the morphology of carotid plaque in three-dimensional ultrasound images [7]. Irregularity in the atherosclerotic plaque border has been quantified by the fractal dimension to be assessed to find its relation to the risk factor [8].

The fractal dimension of a tree depends primarily on the dimensionality of the Euclidean space in which it grows but also on the physical mechanisms that determine its growth. Different pathologies can alter the fractal dimension; therefore, its measurement can have a diagnostic and prognostic value. Variations in the fractal dimension of cardiac signals have been reported related to different pathologies [9–12]. A decrease in the fractal dimension of the eye microvasculature was reported in patients with diabetic retinopathy [13,14].

The fractal dimension can be modified by several geometrical factors such as the boundary conditions when a fractal grows in a limited medium or the existence of a characteristic length, which leads us to consider discrete models such as those used in dielectric breakdown in solids [15]. This last aspect could explain the reported variations in the fractal dimension of the microvascular network of arterioles and venules that were attributed to differences in the dimensions of the vessels [16].

Finally, if a fractal grows on a curved surface (such as a spherical surface), the fractal dimension determined from images or photographs will be influenced by the projection of the surface. Some studies suggest a 3% error in fractal measurements ascribed to retinal curvature [17]. This value can be influenced by the size of the fractal tree.

In this work we study the fractal properties of diffusion-limited aggregation (DLA) clusters generated with particles of different sizes and grown on spherical surfaces. When the particle radius is small compared to that of the sphere, the continuous limit of the model is obtained. Therefore, we study the influence of discretization through the dependence of D_f on r/R, where r is the radius of the particles and R is the radius of the sphere.

The transition to the continuous limit of DLA clusters can be characterized in different forms. Somfai *et al.* [18] used the conformal map method introduced by Hastings and Levitov [19] and employed by Davidovitch *et al.* [20]. The authors proposed a correction to the scale relationships of these fractals that tends to zero when the number of particles tends to infinity. The method was also used in the dielectric breakdown model (DBM), a growth model that can generate clusters with different fractal dimensions, depending on an internal parameter η [21]. The DLA model and the DBM with $\eta = 1$ are equivalent in the continuous limit, because of the relationship between the random-walk and potential theories [15,22]. In the fractal analysis of natural objects, the determination of D_f poses challenges that limit the methods to be used. Though the

*Corresponding author. i_irurzun@hotmail.com.ar

structure of fractals grown under well-controlled conditions or with slow growth can be studied by analyzing the variation of their characteristics with mass, many times fully developed clusters must be studied and the measurements cannot be made as a function of time or the number of particles. This may be the case when analyzing the structure of the retinal microvasculature or dielectric breakdown trees in solids that grow in nanoseconds and are usually detected once generated [23–27]. For this reason, another way of studying the limit to the continuum is to correct the value of D_f, that is, to use D_f as an effective (or apparent) parameter, affected by discretization effects. The latter is the method we use in this work, even though our data can be well described in terms of the crossover proposed by Somfai *et al.* As we discussed above, the usefulness of each description will depend on the possibilities of application in a specific case. What seems important is to know that discretization can appear by modifying the value of D_f and to have a form of correcting these effects knowing that they may not be interpreted as a change in the scale relationship. The growth of DLA aggregates on curved surfaces has also been analyzed [28–30]. In [30] the authors carried out a multifractal analysis in the continuous limit. Our results compare well with them, although we limit ourselves to calculating D_f, which can be compared with D_2 in [30]. A multifractal analysis is beyond the scope of the present work. The conformal map method was extended to DLA clusters grown on cylindrical surfaces with particles of different sizes [29]. The influence of the particle size is qualitatively similar to that reported in this work on spherical surfaces. We also examine the effect of stereographic projection on the fractal dimension and find large deviations.

II. DIFFUSION-LIMITED AGGREGATION MODEL

The DLA model was introduced by Witten and Sanders to describe fractal growth processes dominated by the diffusive transport. It is applicable to many systems such as electrodeposition, Hele-Shaw flow, and dielectric breakdown. The model of Witten and Sander [1] is a variant of the Eden model, whose initial state is a seed particle at the origin of a lattice. In open-plane geometry, this model has a fractal dimension of 1.70 in the continuous limit. Discrete models have to be considered for some physical problems such as the dielectric breakdown phenomenon in solids systems, where the length of the breakdown channel imposes a minimum length. Likewise, the fractal measurement of the circulatory tree has as a minimum length the width of the blood vessels. In discrete models, the fractal dimension depends on both the correlation length and the size of the tree. If the tree grows on a limited surface, such as a sphere, the possible effects of discretization must be considered.

Our purpose is to grow a DLA tree on a spherical surface from the north pole to the south pole. The initial tip is located at the north pole of a sphere of radius 1. The coordinates of this point are $r_i = (0, 0, 1)$, considering the origin of the coordinate system at the center of the sphere. The algorithm follows the following steps.

Step 1. A random walker is launched from the opposite pole where the tip is located. This particle walks randomly until it is actually absorbed by the fractal tree and then added to the tree. To generate a random walker on a spherical surface, it is necessary to carry out the transformation

$$\theta = 2\pi\delta_1, \tag{1}$$

$$\phi = 2\arcsin\sqrt{\delta_2}, \tag{2}$$

where δ_1 and δ_2 are random numbers evenly distributed between 0 and 1. In this way a uniform random distribution is achieved, as shown in Fig. 1.

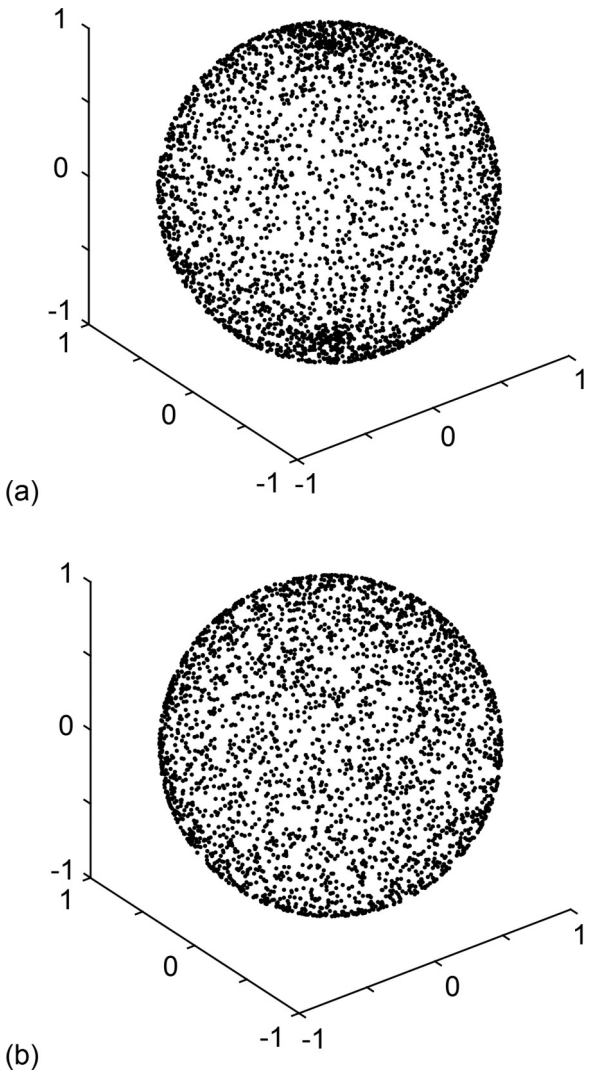

FIG. 1. Uniform random distribution of points on a sphere. (a) Without the transformation given by Eqs. (1) and (2), the points accumulate near the poles. (b) Using Eqs. (1) and (2), a different distribution is achieved.

Step 2. A new random walker is now introduced and it walks randomly until it adheres to the fractal tree and so forth.

Step 3. All particles have the same size r and a particle joins the tree if its distance to any other particle belonging to the structure is equal to or less than $2r$.

Step 4. The particles are rigid; by adhering to the structure, the centers of two joined particles are at a distance equal to $2r$.

FIG. 2. Fractal generated in this work.

The discretization of the system is determined by the value of r. In Fig. 2 we show a fractal generated in this work.

III. STEREOGRAPHIC PROJECTION

The stereographic projection is a particular mapping that projects a sphere onto a plane. The projection is defined on the entire sphere, except at the projection point. Where it is defined, the mapping is smooth and bijective. It is conformal, that is, it preserves angles at which curves meet, but it preserves neither distances nor the areas of figures.

We define below two stereographic projections illustrated in Fig. 3.

Projection A is from the focus $F \equiv (0, 0, f)$ (where $|f|$ is the focal distance) onto the plane $z = 1$, which is tangent to the unit sphere at the north pole [see Fig. 3(a)]. Given $P \equiv (x_p, y_p, z_p)$ a point on the unit sphere and $A = (x_a, y_a, 1)$ its projection on the plane, the transformations that define this projection are

$$x_a = \frac{1-f}{z_p - f} x_p, \tag{3}$$

$$y_a = \frac{1-f}{z_p - f} y_p. \tag{4}$$

Projection B is from the focus $F \equiv (0, 0, f)$ (where $|f|$ is the focal distance) onto the plane $z = p_z$, which is tangent to the unit sphere at the north pole [see Fig. 3(b)]. Given $P \equiv (x_p, y_p, z_p)$ a point on the unit sphere and $A = (x_a, y_a, p_z)$ its projection on the plane, the transformations that define this projection are

$$x_a = \frac{p_z - f}{z_p - f} x_p, \tag{5}$$

$$y_a = \frac{p_z - f}{z_p - f} y_p. \tag{6}$$

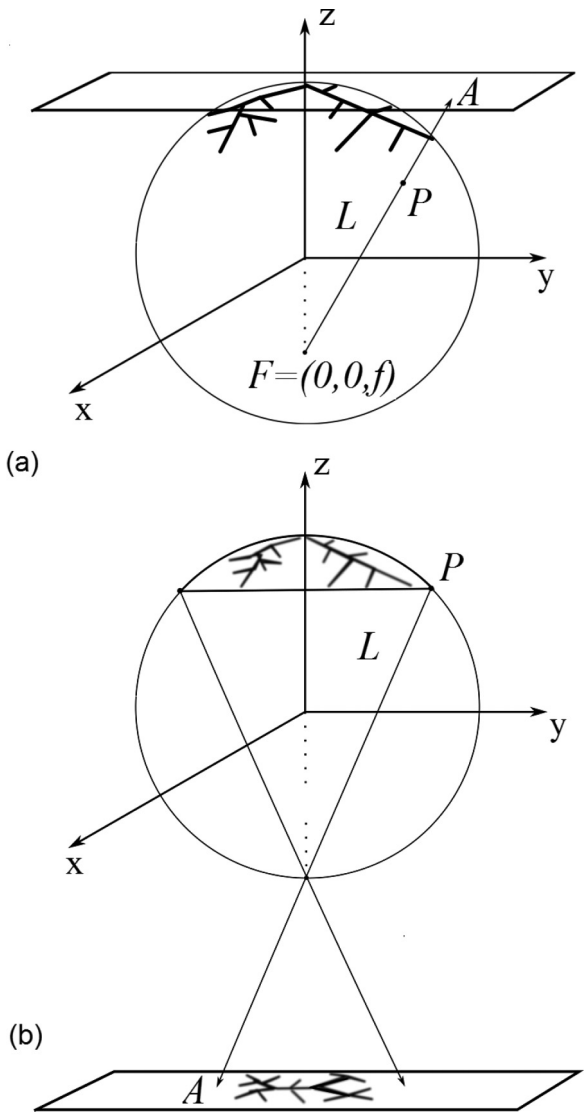

FIG. 3. Stereographic projections: (a) projection A according to Eqs. (3) and (4) and (b) projection B according to Eqs. (5) and (6).

IV. AVERAGE FRACTAL DIMENSION

The simulated fractal trees are structurally characterized by measuring their average fractal dimension D_f. There are different methods to estimate D_f, of which we use two.

Method 1. For the fractal grown on the spherical surface, we consider the relationship between the mass of the tree, M, and its extension, measured as the distance of the furthest particle of the structure to the north pole, L. We calculate M as the number of particles belonging to the tree. The fractal dimension is obtained from the relationship

$$M \propto L^{D_f}. \tag{7}$$

From a log-log plot, an average slope over a set of 250–500 trees (depending on the particle size) is obtained.

Method 2. For stereographic projections, we use the well-known box-counting method. This method counts the number of boxes of size ρ, $N(\rho)$, necessary to cover the fractal structure. The fractal dimension D_f is obtained from the

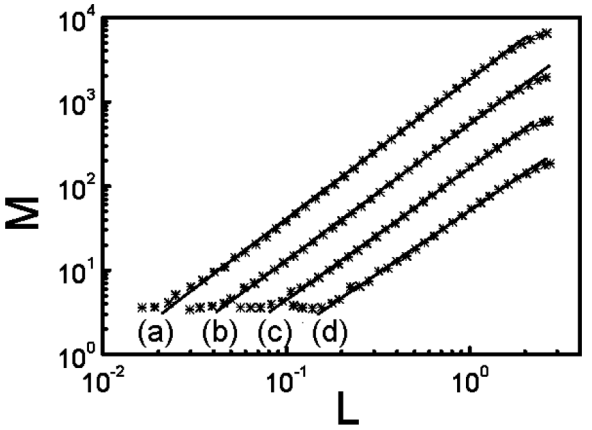

FIG. 4. Plot of M vs L [Eq. (7)] for fractals generated with different particle sizes r with (a) $r^{-1} = 1024$, (b) $r^{-1} = 512$, (c) $r^{-1} = 256$, and (d) $r^{-1} = 128$. See also Fig. 5.

relationship

$$N(\rho) \propto \rho^{-D_f}. \tag{8}$$

Note that ρ indicates the size of the box, while the trees are made up of rigid particles of radius r, as indicated in Sec. II. From a log-log plot, an average slope over a set of 250 trees is obtained.

V. NUMERICAL RESULTS

We consider two possible aspects that can alter the measurements of the fractal dimension D_f: (i) the existence of characteristic lengths that impose a discrete character on the fractal growth and (ii) the existence of projections inherent to the measurement instruments that do not preserve either the distances or the areas of the figures. Below we present the dependence of D_f on the relevant parameters in each case, that is, the size of the particles r and the focal length f.

A. Particle-size effect

Fractal trees are generated with particles of size r such that $r^{-1} \in \{8196, 2048, 1024, 512, 256, 128, 64, 32\}$. The fractals grow on spherical surfaces of radius $R = 1$, according to the algorithm in Sec. II. For each value of r, a set of 250–500 trees is generated (depending on the particle size) and the value of D_f is calculated from Eq. (7). Figure 4 shows some characteristic adjustments to Eq. (7). Figure 5 shows the dependence of D_f on r. The limit value $D_f = 1.70$ is reached at $r = \frac{1}{2048}$.

This limit value coincides with that reported in [30]. The authors report that the fractal dimension D_f is insensitive to the surface curvature. This is because the surface is locally Euclidean if the particle size is small enough. If the size of the particles increases, the effects of the discretization become evident with an apparent decrease in D_f or in the slope in a log-log plot of Eq. (7). These results qualitatively agree with those presented in [29] on a cylindrical surface.

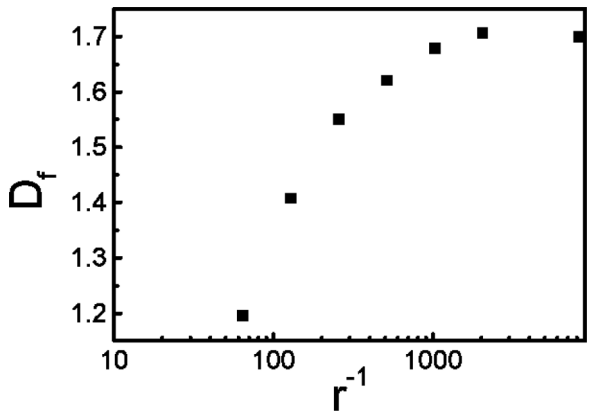

FIG. 5. Plot of the D_f dependence on the particle size.

B. Stereographic projection

To study the effect of the projection, we consider the trees generated with $r = \frac{1}{8196}$. Figure 6 shows the projections of a tree grown on a spherical surface, according to Eqs. (3) and (4) (projection A) with different f values. The fractal dimension D_f is determined according to Eq. (8).

The effects of projection A (Sec. III) are studied by determining the dependence of D_f on f, as shown in Fig. 7. The D_f values approach 1.70 as $|f|$ increases, but even with $|f| = 4$, the D_f values are significantly lower than 1.70.

The effects of projection B are studied qualitatively as a function of the angle α defined in Fig. 3(b). The fractal dimension D_f decreases as α increases, 2% for $\alpha = 45$ and 5% for $\alpha = 90$. In this projection, a relationship must be established between the distance to the projection plane and the latitudinal extension of the fractal.

VI. DISCUSSION AND CONCLUSIONS

In this work we generate and study DLA clusters on spherical surfaces with particles of different sizes. In two-dimensional media, DLA fractals have a fractal dimension

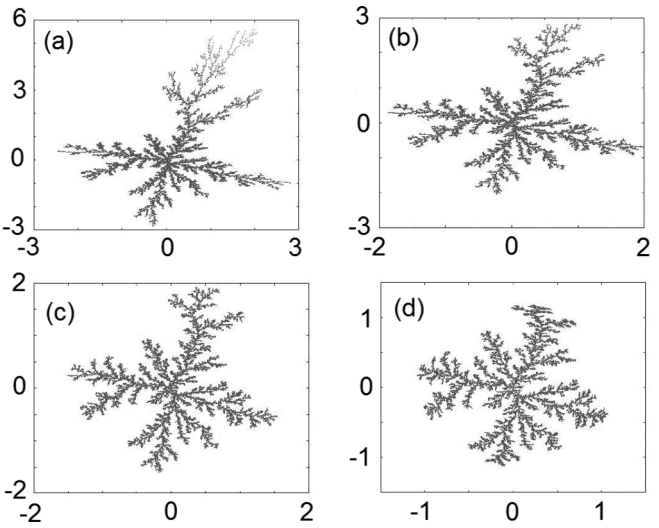

FIG. 6. Stereographic projection A of a fractal generated on a spherical surface using different focal lengths (a) $f = -0.2$, (b) $f = -0.5$, (c) $f = -1$, and (d) $f = -2$.

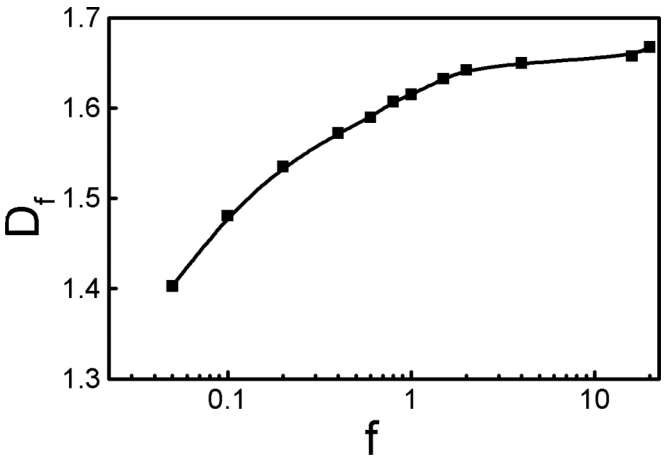

FIG. 7. Plot of the D_f dependence on $|f|$.

$D_f = 1.70$ in the continuous limit [29,30]. The existence of characteristic lengths forces us to consider discrete models for some physical systems. Such lengths can also result from limitations in measuring instruments, for example, the resolution of photographic images. Thus, the finite nature of the spherical surface leads to exploring discrete models in terms of the relationship between the characteristic length (or particle size) and the radius of the sphere R. In this work we determine that the continuous limit is reached for particles of size $r = R/2048$. This result would determine the resolution of the biomedical images in which discretization is negligible.

The transition to the continuous limit of DLA clusters was studied by Somfai *et al.* as a slow crossover towards the asymptotic scaling behavior for large values of M. They proposed a correction to the scale relationships of these fractals that tend to zero when the number of particles tends to infinity and can be written as

$$\frac{L^2}{M^{2/D_f}} = \alpha + \beta M^{-\phi}. \tag{9}$$

Values of L can be appropriately normalized so that $\boldsymbol{\alpha = 1}$. Furthermore $\boldsymbol{D_f = 1.70}$ and $\boldsymbol{\phi = 0.3 \pm 0.1}$, as was determined in [30] in a Euclidean geometry. Our data satisfy Eq. (9) with the same $\boldsymbol{\phi}$ value, as shown in Fig. 8. Now the $\boldsymbol{\beta}$ values depend on the particle size as was also observed in [29] on a cylindrical surface (this effect was not studied on a spherical surface). The use of Eq. (9) in practical situations can be difficult. As we explained above, there are situations in which it is not possible to carry out studies based on M, but it should still be possible to use fractal features to characterize irregular objects. In these situations using D_f as a parameter to characterize the effects of discretization, as was done in this work, is preferable.

Also, the projection of the fractal alters its dimension. We explored stereographic projection and found that the farther away the projection plane is from the sphere, the better the estimate of the fractal dimension. For the stereographic projection A with $|f| = 1$, the D_f values are 6% lower, a difference greater than those attributed to various pathologies. In the stereographic projection B, the deviations depend on α, which should not exceed 45.

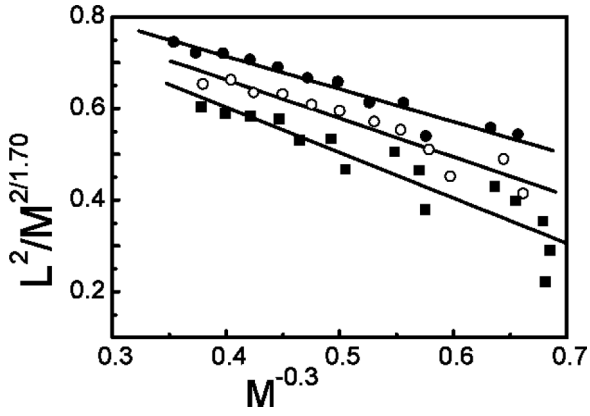

FIG. 8. Transition to the continuous limit according to Eq. (9) for fractals generated with different particle sizes r. Closed circles represent $r^{-1} = 1024$ and $\beta = -0.72 \pm 0.05$, open circles $r^{-1} = 512$ and $\beta = -0.84 \pm 0.06$, and closed squares $r^{-1} = 256$ and $\beta = -1.0 \pm 0.1$. Here L is normalized so that $\alpha = 1$ in Eq. (9).

The effects of the projection must be considered in the analysis of ophthalmological images of the blood vessels of the eye. In these cases, the projection plane can be very close to the eyeball. Furthermore, the type of projection may change depending on the relative location of the fractal being analyzed. Many studies have attempted to relate variations of the fractal dimension to pathological alterations that affect the growth dynamics of the circulatory network. However, the effects of finite size and the effects of the projection must be considered to compare the results with each other and give them a diagnostic value.

For example, the fractal dimension D_f is being used to characterize the retinal vasculature in patients with diabetic retinopathy. Fan *et al.* [17] measured the D_f of the retinal vasculature in both healthy (control) eyes and diabetic retinopathic eyes. The authors obtained ultrawide field fluorescence angiography images of 4000×4000 pixels, although the characteristic length is three to four pixels, corresponding to the width of the vessels. Therefore, the D_f values may be affected by the discrete nature of the fractal. The authors reported values of $D_f = 1.6 \pm 0.04$ for the healthy (control) eye. These values are comparable to D_f values for a discrete DLA fractal with $r = R/1024$ (Fig. 5). Their regional analysis indicated that diabetic retinopathic eyes had a lower D_f in the far periphery compared to healthy controls. The D_f values for healthy controls decreased by 5% between the posterior region and the midperiphery, corresponding to values of $\alpha < 45$ and $45 < \alpha < 90$ in a type B stereographic projection, such as that used in [17]. These results are again comparable to our calculations on DLA fractals. The retina vasculature of the healthy eye therefore may have a DLA fractal structure and the reported variations may be due to factors such as discretization and projection. Our work provides a theoretical reference (noise-free) to distinguish these effects.

ACKNOWLEDGMENTS

This research project was financially supported by the National Research Council of Argentina, Grant No. PIP 0062 and the National University of La Plata, Grant No. 11/X874.

[1] B. Smitha and K. Paul Joseph, Chaos Soliton. Fract. **123**, 91 (2019).

[2] B. B. Mandelbrot, *The Fractal Geometry of Nature* (Freeman, New York, 1983).

[3] R. Xu, Y. Sun, Z. Yang, B. Song, and X. Hu, IEEE Trans. Nanobiosci. **14**, 513 (2015).

[4] M. Z. C. Azemin, D. K. Kumar, T. Y. Wong, R. Kawasaki, P. Mitchell, and J. J. Wang, IEEE Trans. Med. Imag. **30**, 243 (2011).

[5] G. Verma, M. L. Luciani, A. Palombo, L. Metaxa, G. Panzironi, F. Pediconi, A. Giuliani, M. Bizzarri, and V. Todde, Comput. Biol. Med. **93**, 1 (2018).

[6] E. Akar, H. Akdemir, and K. Adem, Comput. Biol. Med. **64**, 179 (2015).

[7] R. Zhou, Y. Luo, A. Fenster, J. D. Spence, and M. Ding, Med. Biol. Eng. Comput. **57**, 135 (2019).

[8] G. Camici, PLoS One **13**, e0192600 (2018).

[9] I. M. Irurzun, P. Bergero, M. C. Cordero, M. M. Defeo, J. L. Vicente, and E. E. Mola, Chaos Soliton. Fract. **16**, 699 (2003).

[10] D. S. Andrés, I. M. Irurzun, J. Mitelman, and E. E. Mola, Appl. Phys. Lett. **89**, 144111 (2006).

[11] I. M. Irurzun and E. E. Mola, *Heart Rate Variability: A View from Chaos Theory* (Lambert, Saarbrücken, 2015).

[12] A. Voss, R. Schroeder, A. Heitmann, A. Peters, and S. Perz, PLoS One **10**, e0118308 (2015).

[13] Z. Sun, F. Tang, R. Wong, J. Lok, S. K. H. Szeto, J. C. K. Chan, C. K. M. Chan, C. C. Tham, D. S. Ng, and C. Y. Cheung, Ophthalmology **126**, 1675 (2019).

[14] F. Y. Tang, D. S. Ng, A. Lam, F. Luk, R. Wong, C. Chan, S. Mohamed, A. Fong, J. Lok, T. Tso, F. Lai, M. Brelen, T. Y. Wong, C. C. Tham, and C. Y. Cheung, Sci. Rep. **7**, 2575 (2017).

[15] I. M. Irurzun, P. Bergero, V. Mola, M. C. Cordero, J. L. Vicente, and E. E. Mola, Chaos Soliton. Fract. **13**, 1333 (2002).

[16] R. Wang, P. Li, Q. Pan, J. K. Li, W. M. Kuebler, A. R. Pries, and G. Ning, Microvasc. Res. **125**, 103882 (2019).

[17] W. Fan, M. G. Nittala, A. Fleming, G. Robertson, A. Uji, C. C. Wykoff, D. M. Brown, J. van Hemert, M. Ip, K. Wang, K. G. Falavarjani, M. Singer, M. Sagong, and S. R. Sadda, Am. J. Ophthalmol. **209**, 99 (2020).

[18] E. Somfai, L. M. Sander, and R. C. Ball, Phys. Rev. Lett. **83**, 5523 (1999).

[19] M. B. Hastings and L. S. Levitov, Physica D **116**, 244 (1998).

[20] B. Davidovitch, H. G. E. Hentschel, Z. Olami, I. Procaccia, L. M. Sander, and E. Somfai, Phys. Rev. E **59**, 1368 (1999).

[21] J. Mathiesen, M. H. Jensen, J. Ø. H. Bakke, Phys. Rev. E **77**, 066203 (2008).

[22] L. Pietronero and H. J. Wiesmann, J. Stat. Phys. **36**, 909 (1984).

[23] I. M. Irurzun, J. L. Vicente, M. C. Cordero, and E. E. Mola, Phys. Rev. E **63**, 016110 (2000).

[24] R. Schurch, J. Ardila-Rey, J. Montana, A. Angulo, S. M. Rowland, and I. Iddrissu, IEEE Trans. Dielectr. Electr. Insul. **26**, 220 (2019).

[25] A. Colomer, V. Naranjo, T. Janvier, and J. M. Mossi, J. Comput. Appl. Math. **337**, 341 (2018).

[26] L. Salvatierra, L. Kovalevski, P. L. Dammig Quiña, I. M. Irurzun, E. E. Mola, S. J. Dodd, and L. A. Dissado, IEEE Trans. Dielectr. Electr. Insul. **23**, 757 (2016).

[27] F. L. Ribeiro, R. Vieira dos Santos, and A. S. Mata, Phys. Rev. E **95**, 042406 (2017).

[28] B. Kol and A. Aharony, Phys. Rev. E **58**, 4716 (1998).

[29] A. Taloni, E. Caglioti, V. Loreto, and L. Pietronero, J. Stat. Mech. (2006) P09004.

[30] J. Choi, D. Crowdy, and M. Z. Bazant, Europhys. Lett. **91**, 46005 (2010).